Origin and distribution of charge carriers in $LaAlO_3$-$SrTiO_3$ oxide heterostructures in the high carrier density limit

Sumanta Mukherjee and Banabir Pal
Solid State and Structural Chemistry Unit, Indian Institute of Science, Bengaluru 560012, India

Debraj Choudhury
Solid State and Structural Chemistry Unit, Indian Institute of Science, Bengaluru 560012, India
and Department of Physics, Indian Institute of Technology Kharagpur, Kharagpur 721302, India

Indranil Sarkar and Wolfgang Drube
Deutsches Elektronen-Synchrotron DESY, Notkestrasse 85, D-22607 Hamburg, Germany

Mihaela Gorgoi
Helmholtz Zentrum Berlin für Materialien und Energie GmbH, Albert Einstein Straße 15, 12489 Berlin, Germany

Olof Karis
Department of Physics and Astronomy, Box 516, 75120 Uppsala, Sweden

H. Takagi
Department of Physics, University of Tokyo, Tokyo 113-0033, Japan
and Max-Plank-Institute for Solid State Research, Stuttgart 70569, Germany

Jobu Matsuno
RIKEN Center for Emergent Matter Science (CEMS), Saitama 351-0198, Japan

D. D. Sarma*
Solid State and Structural Chemistry Unit, Indian Institute of Science, Bengaluru 560012, India;
Department of Physics and Astronomy, Box 516, 75120 Uppsala, Sweden;
and Council of Scientific and Industrial Research - Network of Institutes for Solar Energy (CSIR-NISE), New Delhi 110001, India

(Received 14 May 2015; revised manuscript received 28 April 2016; published 10 June 2016)

Using hard x-ray photoelectron spectroscopy with variable photon energy (2–8 keV), we address the distribution of charge carriers in the prototypical $LaAlO_3$ (LAO) and $SrTiO_3$ (STO) oxide heterostructures with high carrier densities (10^{17} cm^{-2}). Our results demonstrate the presence of two distinct charge distributions in this system: one tied to the interface with a ∼1-nm width and ∼2–5 × 10^{14}-cm^{-2} carrier concentration, while the other appears distributed nearly homogeneously through the bulk of STO corresponding to a much larger carrier contribution. Our results also establish bimodal oxygen vacancies, namely on top of LAO and throughout STO, quantitatively establishing these as the origin of the observed bimodal depth distribution of charge carriers in these highly doped sample.

DOI: 10.1103/PhysRevB.93.245124

I. INTRODUCTION

The presence of highly mobile two-dimensional electron gas (2DEG) [1,2] at the interface of two insulating, diamagnetic oxides $LaAlO_3$ (LAO) and $SrTiO_3$ (STO) has opened up a new field of research [3,4]. Despite many reports on remarkable properties of this apparently simple oxide interface [2,5–11] the appropriate description of this interface has remained controversial [1,12–23]. Even the very central question, whether a single type of charge carriers is responsible for all these, at times, apparently mutually exclusive properties [8,22], has not found a satisfactory answer. In its simplest generic form, the increasing polar field in the overlayer LAO with an increasing thickness can be compensated by the transfer of half an electron per formula unit from the topmost layer of LAO to the topmost TiO_2 layer of STO at the interface [1,12]; this implies the existence of a two-dimensional electron gas with a density of 3.28×10^{14} cm^{-2} at the interface. Extensive first-principles calculations suggest a typical thickness of ∼2 nm for the thus formed 2DEG [24,25]. It is also understood now that the polar discontinuity across the interface of LAO-STO heterostructures can be resolved by a combination of various electronic and atomic reconstructions as well as vacancies, thereby leading to a wide range of electron densities varying from 10^{12}–10^{17} cm^{-2}, with significant changes in the transport and magnetic properties [2,4,7]. Moreover, many estimates [1,5,10,11,17,26–30] of the thickness of the 2DEG

*Also at Jawaharlal Nehru Centre for Advanced Scientific Research, Bengaluru 560064, India; sarma@sscu.iisc.ernet.in

are inconsistent with the idea of the mobile charge carriers being present only at a very narrow region (of the order of few nm) at the interface [12,31]. Not only have the charge-carrier density and its spatial distribution remained a popular topic, the nature of the charge carriers at the interface has also been unclear so far [4,8,30,32–36]. Hall measurements on samples with a density of carriers of $\approx 10^{13}\text{cm}^{-2}$ or more are inconsistent with the idea of a single charge distribution [7,11,37]. Optical conductivity measurements [30,34,35] also indicate the presence of two different types of charge carriers—one high mobility, low carrier density coexisting with a high carrier density distribution with much lower mobility. There are several different attempts to rationalize these observations [9,18,33,38–40].

We performed hard x-ray photoelectron spectroscopy (HAXPES) studies to unravel the origin and depth distribution of the charge carriers in this prototypical oxide based 2DEG system. We have used varying photon energy between 2 and 8 keV, that gives a large information depth extending up to ∼25 nm, giving access to the electronic structure of STO deep in the heterostructure. The advantages of this technique are obvious for studies of buried interfaces, and heterostructures in general [41–46], compared to cross-sectional microscopy-based approaches that are invasive and necessarily introduce an additional vacuum-heterostructure interface. Photoelectron spectroscopy has previously been used to probe LAO/STO heterostructures, resulting in conflicting conclusions [21,28,47,48], possibly attributable to the more limited mean free path of photoelectrons in those experiments (1.1–3 nm). By fully utilizing the merits of HAXPES, we obtained electronic structure information deeper into the heterostructure and show for samples with high electron densities (10^{17} cm^{-2} by Hall measurements) that (i) there are two distinct electronic charge-carrier distributions in this system: one tied to the interface and the other relatively homogeneous and extended deeper into the STO layer; and (ii) the origin of these two distributions are found to be related to the oxygen vacancy distribution and band bending at the interface. The total Ti 3*d* doped charge seen in our experiment amounts approximately to $5–10\times10^{14}$ cm^{-2} due to the much smaller probing depth compared to Hall measurements.

II. EXPERIMENTAL SECTION

n-type interfaces between STO and LAO were grown by means of pulsed laser deposition (PLD) of LAO on TiO_2 terminated STO single crystal at two different oxygen pressures ($pO_2 \sim 10^{-4}$ Torr and $pO_2 \sim 3\times10^{-7}$ Torr), with a laser fluence of ∼2 J cm^{-2} respectively. The STO substrates were heat treated at 900 °C at these oxygen pressures, prior to deposition of the LAO. Two different LAO thicknesses [4 and 6 unit cells (uc)] were grown, giving four samples denoted as 4H, 4L, 6H, and 6L, respectively, keeping in mind the critical thickness for metallicity being 4 uc [2] and the LAO thickness dependent properties [49]. The numbers indicate the LAO thickness in uc, while H and L represent the high and low oxygen pressures during growth, respectively. A representative cross-sectional transmission electron microscope (TEM) image of the 6L sample is shown in Fig. 1(a), illustrating growth of pseudomorphic LAO on top of STO. The sheet resistance as a function of the temperature of three samples is given in Fig. 1(b). Resistance and Hall measurements establish the expected metallic behavior of 6H, 6L, and 4L samples with carrier concentrations of $\sim2\times10^{13}$ cm^{-2}, $\sim2\times10^{17}$ cm^{-2} and $\sim2\times10^{17}$ cm^{-2} respectively. For the 4H sample the sample resistance was found to be larger than our measurement range; however the sample did not to show any charging effect in HAXPES measurements, indicating sufficient conductivity to neutralize the photocurrent, but with a carrier concentration lower than 2×10^{13} cm^{-2}. Since our technique cannot detect a charge-carrier density lower than $\sim5\times10^{13}$ cm^{-2}, as explained later in the text, samples 4H and 6H provide references for essentially undoped samples for all practical purposes without the usual complication of charging effects usually observed for insulating samples. This allows us to map the charge distributions of the higher doped 4L and 6L samples, respectively. HAXPES measurements were performed at the HIKE experimental station at KMC-1 bending magnet beam line at the Helmholtz-Zentrum, Berlin [50] and at the HAXPES end station P09 of the Petra-III beamline, DESY, Hamburg, Germany [43], using photon energies between 2 and 8 keV. The base pressure was in the low 10^{-9} mbar range at both facilities. We have used the binding energy (BE) of the C

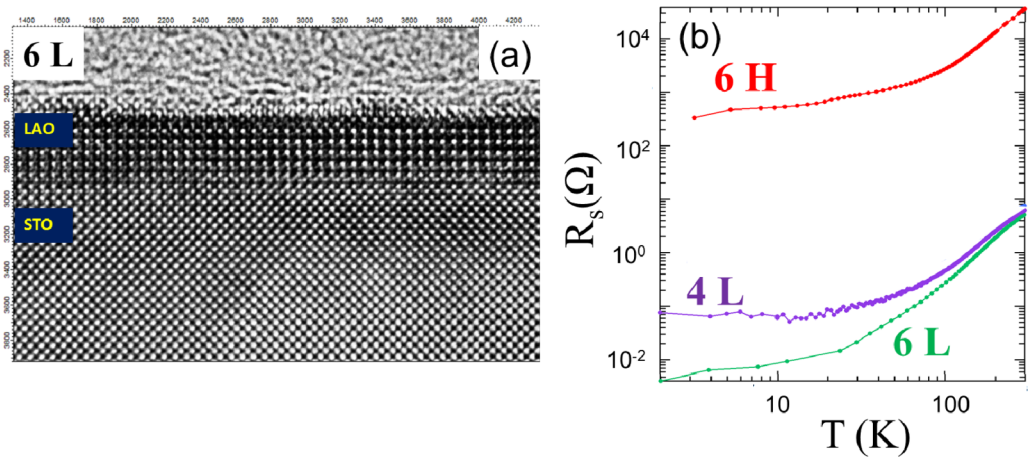

FIG. 1. (a) Cross-sectional TEM image of 6L sample. (b) Sheet resistance as a function of temperature for 6H, 4L, and 6L samples.

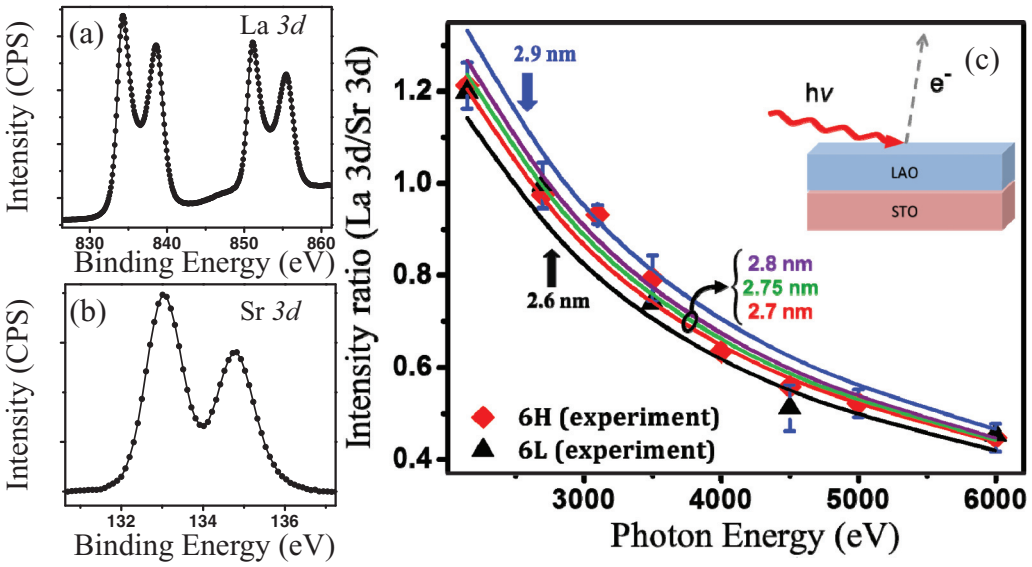

FIG. 2. (a), (b) La 3*d* and Sr 3*d* core-level spectra recorded with a incident photon energy of 3500 eV. (c) Cross-section and transmission function corrected experimental intensity ratios between La 3*d* and Sr 3*d* core-level spectra as a function of photon energy for 6H and 6L samples along with the calculated variations in this intensity ratio obtained for different LAO thicknesses as shown.

1*s* core level, corrected for recoil effects [51], as the internal reference for calibration of photon energies.

III. RESULTS AND DISCUSSION

To address the possibility of intermixing at the LAO/STO interface, we recorded La 3*d* and Sr 3*d* core-level spectra at various incident photon energies. Two representative spectra of La 3*d* and Sr 3*d* core levels recorded with 3500-eV photon energies are shown in Figs. 2(a) and 2(b), evidencing clean spectral features and an absence of any contaminants. We estimated the cross-section and transmission function corrected intensity ratio of La 3*d* and Sr 3*d* core levels as a function of the photon energy, shown for 6L (diamonds) and 6H (triangles) samples in Fig. 2(c). Following the quantitative analysis reported earlier [41,42,52,53], we express the La 3*d*/Sr 3*d* intensity ratio as a function of the photon energy as

$$\frac{I_{\mathrm{La}}(h\nu)}{I_{\mathrm{Sr}}(h\nu)} = \frac{\sigma_{\mathrm{La}}(h\nu)}{\sigma_{\mathrm{Sr}}(h\nu)} \frac{\int_\theta T(\mathrm{KE},\theta) \int_0^\infty n_{\mathrm{La}}(z) \exp\left[-z/\{\lambda_{\mathrm{La}}(\mathrm{KE},\theta)\cos\theta'\}\right] dz d\theta}{\int_\theta T(\mathrm{KE}',\theta) \int_0^\infty n_{\mathrm{Sr}}(z) \exp\left[-z/\{\lambda_{\mathrm{Sr}}(\mathrm{KE}',\theta)\cos\theta'\}\right] dz d\theta}, \tag{1}$$

where KE is the kinetic energy of the photoelectrons, σ is the photoionization cross section, λ is the photoelectron mean free path, θ' is the photoelectron emission angle, and θ is the angle of acceptance of the analyzer. T is the analyzer transmission function, $n(z)$ is the depth (z) dependent number density of an element within the heterostructure in the surface-normal direction. In Fig. 2(c) we plot the calculated dependence of this intensity ratio on photon energy for several fixed values of the LAO thickness between 2.6 and 2.9 nm. Comparison of these plots with the experimental data convincingly demonstrates the sensitivity of the technique. A LAO thickness of either 2.6 or 2.9 nm would be clearly inconsistent with the experiment and that the LAO layer with a sharp interface is consistent only with a thickness of 2.75 ± 0.05 nm [54]. Allowing for various models of interdiffusion of La and Sr across the interface, we find that any such intermixing has to be limited to within a single atomic layer, consistent with Fig. 1(a).

Figure 3(a) shows Ti 2*p* spectra of the four samples recorded using 3500-eV photon energy. The main spectral features with peaks at 459.2 and 465 eV binding energies (BE's) correspond to the spin-orbit split 2*p* level of Ti^{4+} of $SrTiO_3$ [28,47,55]. The Ti 2*p* spectra of 4L and 6L samples show an additional peak at 457 eV BE. Comparing with reference samples, this feature can be assigned to the electron doping of Ti 3*d* levels, giving rise to Ti^{3+} species [28,47,55]. By constructing spectral features for the Ti^{3+} signal at various doping levels, we find that the corresponding intensity is below the detection limit for carrier concentration of $\sim 5 \times 10^{13}$ cm^{-2} for 6 and 4 uc LAO samples, assuming that the entire doping is confined within one unit cell at the interface, explaining the absence of the Ti^{3+} signal in 6H and 4H samples. We separate Ti^{3+} and Ti^{4+} contributions to the total Ti 2*p* spectrum by spectral decomposition, as shown in Fig. 3(b). The ratio of the total intensities of the two components, Ti^{3+} and Ti^{4+}, is a measure of the fraction of electron doping of Ti 3*d* states as probed in photoemission experiments. Since the photoemission probing depth increases monotonically with increasing photon energy, we monitor the Ti^{3+}/Ti^{4+} intensity

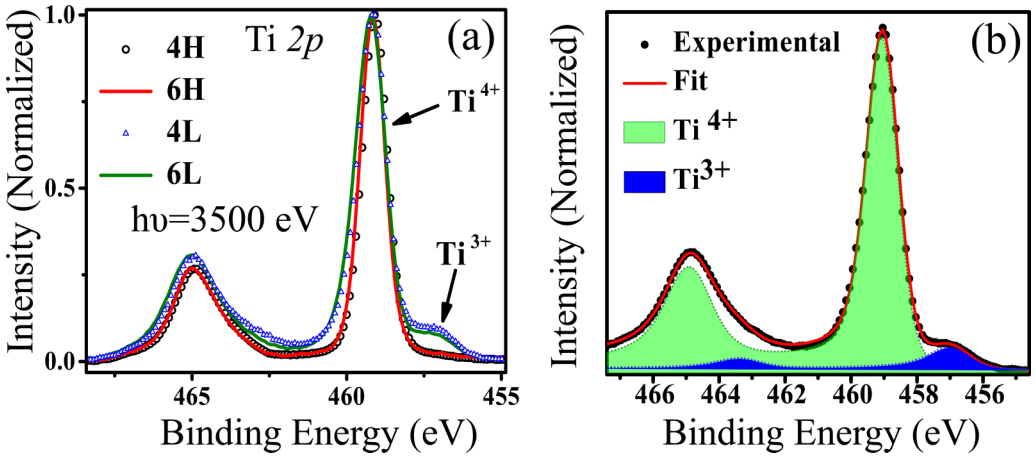

FIG. 3. (a) Ti $2p$ x-ray photoelectron spectra of 4H, 4L, 6H, and 6L samples recorded with photon energy of $h\nu = 3500$ eV. (b) Illustration of a typical spectral decomposition of Ti $2p$ spectra in terms of Ti^{4+} and Ti^{3+} components.

ratio for all samples as a function of photon energy. The Ti^{3+}/Ti^{4+} intensity ratios for both 4L and 6L samples decreases with increasing photon energy, as shown by filled diamonds in Figs. 4(a) and 4(b), respectively. The dependence of the Ti^{3+}/Ti^{4+} intensity ratio on the photon energy is determined by the depth distribution of the doped electrons, enabling us to extract the distribution of the carriers from the experimental data presented in Figs. 4(a) and 4(b) following an analysis analogous to that presented for the La $3d$/Sr $3d$ variation. We find that a single charge distribution at the LAO/STO interface is insufficient to provide a reasonable description of the energy dependence of the Ti^{3+}/Ti^{4+} intensity ratio. The best fits of a model with single charge distribution, for 4L and 6L samples, are shown as a dashed line in the

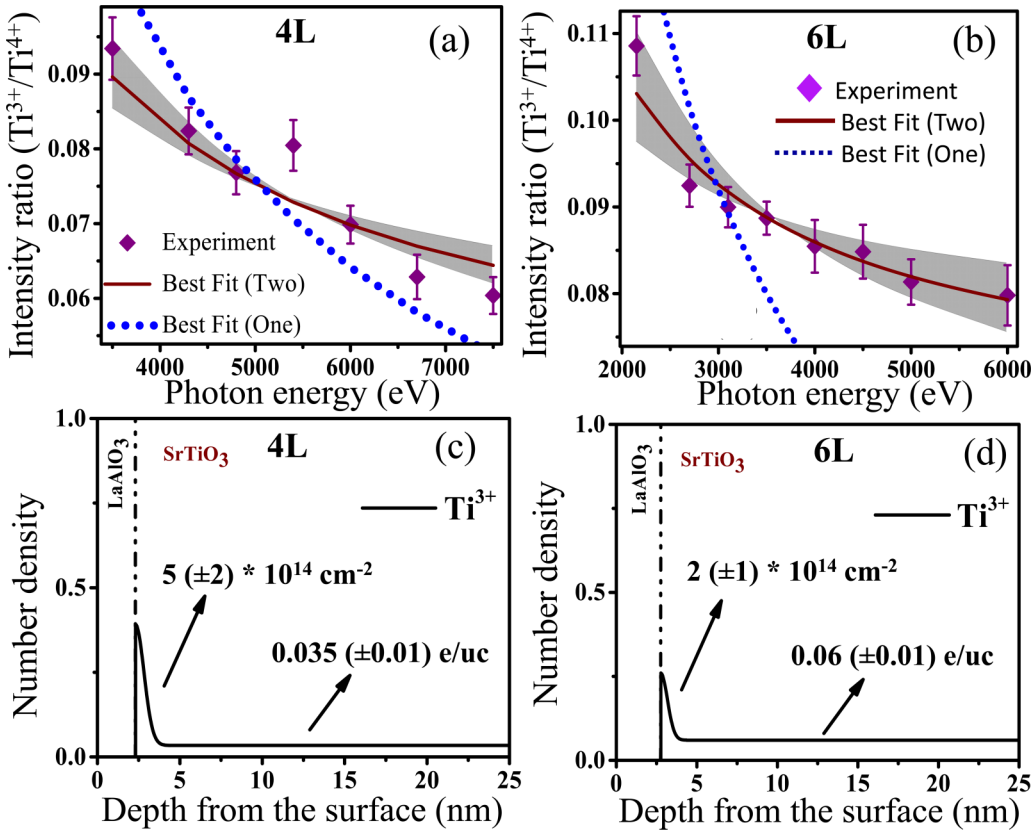

FIG. 4. (a) and (b) Ti^{3+}/Ti^{4+} intensity ratio as a function of the photon energy for 4L and 6L samples. Dotted and solid lines represent different fits to these intensity ratio with different models having single and bimodal charge distribution, respectively. (c) and (d) Charge carrier distributions that provide the best fit to the Ti^{3+}/Ti^{4+} intensity ratios, shown for 4L and 6L samples, respectively. The vertical dash-dotted line represents the interface, as obtained from the simulation of the La $3d$/Sr $3d$ intensity ratio. Values of uncertainties on different numbers in (c) and (d) are obtained from extremal fits to the experimental data in Figs. (a) and (b), as shown by the shaded regions.

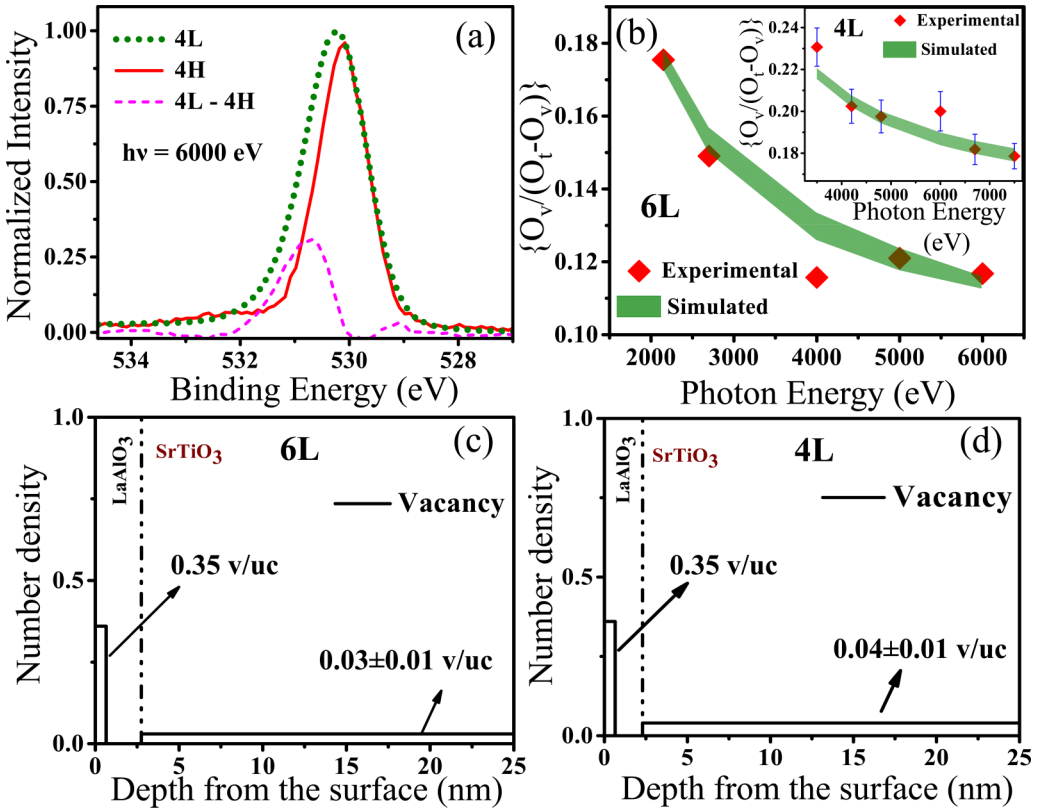

FIG. 5. (a) O 1s photoelectron spectra with $h\nu = 6000$ eV for 4L (dotted line) and 4H (solid line). The difference spectrum is shown by the dashed line. (b) Experimentally obtained (diamonds) and simulated (shaded) intensity ratios between oxygen vacancy related peak (O_v) with respect to the rest of the oxygen spectra (O_t-O_v) for 6L. The inset shows the same for 4L. (c),(d) Oxygen vacancy distributions (solid lines) deduced from the experimental intensity ratios in (b), for 6L and 4L samples, respectively.

Figs. 4(a) and 4(b) [56], respectively. Instead, we find that a description of the charge-carrier density in terms of two distributions provides a very good fit to the experimental data. While other functional forms work nearly as well, we illustrate the results obtained with a Gaussian distribution near the interface and a constant charge-carrier density extending deeper into the STO layer as solid lines in Figs. 4(a) and 4(b). The corresponding distributions of charge carriers are shown as the solid lines in Figs. 4(c) and 4(d) for the 4L and 6L, respectively. The best agreement with the experimental data requires one charge-density distribution at the LAO/STO interface with a width of ~1 nm into STO and a charge-carrier density of $\sim(5 \pm 2)\times10^{14}$ cm^{-2} and $\sim(2 \pm 1)\times10^{14}$ cm^{-2} for 4L and 6L, respectively. These numbers are in agreement with those proposed from confinement of carriers from the band-bending scenario at LAO-STO [21] or at STO-vacuum interfaces [57–60]. We also require a second distribution with a lower density extending into $SrTiO_3$ up to a depth of ~25 nm or more [61]. We choose to specify the carrier density for this distribution in terms of the numbers of doped electrons (~0.03–0.06) per uc of STO rather than converting it into a two-dimensional charge density, owing to the nature of the distributions (3D rather than 2D). Taking into account the exponentially decaying contributions to the spectral intensity from deeper layers [see, e.g., Eq. (1)] and typical mean free paths, we estimate that the total integrated charge density observed in our photoelectron measurements is in the order of ~5–10×10^{14} cm^{-2}, including a roughly equal contribution from the charge carriers associated with the LAO/STO interface and those distributed within STO. In order to be consistent with the observed total charge-carrier density from volume averaging Hall measurements, namely $\sim2\times10^{17}$ cm^{-2}, the 0.03–0.06-e/uc doped region of STO needs to be ~1 μm thick. While no photoemission measurement can probe this deep, this width is consistent with the estimate of a 100-nm doped layer from calculations of oxygen vacancy distributions [14]. We recall that both the samples (4L and 6L) that show evidence of mobile charge carriers are synthesized at a low oxygen pressure $pO_2 \sim 3\times10^{-7}$ Torr. This is expected to give rise to oxygen vacancies in $SrTiO_3$ [4,7,14,17,36,62,63].

In order to address this issue, we compare the O 1s photoelectron spectra in Fig. 5(a) for the 4L (dotted line) and 4H (solid line) samples. The spectrum for the 4L sample is clearly showing a broadening towardsthe higher BE side. Forming a difference spectrum from the two O 1s spectra reveals the presence of a feature at 530.7 eV, shown by the dashed line in the same figure. We relate this peak to the nearest-neighbor oxygen ions surrounding an oxygen vacancy. We have estimated the intensity of this vacancy induced feature (O_v) at various photon energies by subtracting the oxygen intensity of the high pressure grown samples from the total oxygen intensity (O_t) of the low pressure grown sample at each photon energies. The variation of relative intensity ratio of this peak (O_v) with respect to the rest of the O 1s spectrum (O_t-O_v), as a function of

the incident photon energy is shown for the 6L and 4L samples in the main panel and the inset of Fig. 5(b), respectively. Following an analogous analysis as for the Ti $2p$ spectra, we obtain the oxygen vacancy distribution within the LAO and STO layers as shown in Figs. 5(c) and 5(d) with solid lines for 6L and 4L samples, respectively. Again we need a minimum of two separate distributions of oxygen vacancies to describe the experimental intensity ratios. The best description is shown by the thick shaded lines in Fig. 5(b). One distribution of vacancies is found within the STO layer. This could be best modeled by a homogeneous distribution within the probing depth, corresponding to an average composition of $SrTiO_{2.97}$ and $SrTiO_{2.96}$ for 6L [Fig. 5(c)] and 4L [Fig. 5(d)]. A concentration of oxygen vacancies of 0.03 (0.04) per formula unit will dope the system with 0.06 (0.08) electrons per unit cell of 6L (4L). This is in good agreement with the independently estimated number of homogeneously doped charge carriers from our analysis of the Ti $2p$ spectra above, namely 0.06 and 0.035 electrons per unit cell for 6L and 4L, respectively. This correlation lends strong support to the proposition that oxygen vacancies are the origin of the extended carrier distribution within the STO substrate. While some part of these carriers, generated due to the presence of extensive oxygen vacancies within STO, can provide enough electrons to populate the spatially confined conduction band close to the LAO-STO interface, thereby explaining the origin of both the charge-carrier distributions [Figs. 4(c) and 4(d)] [21], the best-fit model for the experimentally observed intensity variations [Fig. 5(b)] required the presence of an additional oxygen vacancy distribution confined within the topmost unit cells of $LaAlO_3$ to explain the photon energy dependence. Since we have a homogeneous model, $n(z)$, to describe the distribution, it is not possible to delineate with confidence the presence of this oxygen vacancy among the top few layers. However, the best-fit data for this distribution, shown in Figs. 5(c) and 5(d), correspond to a thickness of $\sim$0.65 nm, indicating oxygen vacancies predominantly in the top two unit cells. For both 6L and 4L samples, oxygen vacancy concentrations are $\sim$0.35 per unit cell, corresponding to an electron doping of $\sim$0.7 per unit cell, or in other words $\sim 5\times10^{14}$ cm^{-2} carriers. This number is the same within the uncertainty, as the charge-carrier concentration obtained at the LAO/STO interface from the analysis of Ti $2p$ spectral features [Figs. 4(c) and 4(d)]. This suggests that the carriers at the interface arise due to the presence of vacancies at the topmost LAO surface. It is interesting to note here that there are two independent theoretical reports here [64,65] that did suggest exactly this scenario of charge-carrier doping via oxygen vacancy formation at the top-most LAO layer as the required by energy stability. These have been largely overlooked to date, likely due to the absence of any experimental evidence so far. Our results on the other hand provide direct evidence for the formation of oxygen vacancies in the LAO layer. We also note that there is no evidence, so far, of metallicity for the top LAO layer, while such a metallic layer would be a consequence of transferring half an electron to the interface from the LAO top layer, thereby doping holes in the LAO layer. Formation of oxygen vacancies at the top layer will counteract hole doping of the LAO layer.

IV. CONCLUSION

In conclusion, photoemission experiments with photon energy ranging up to 8 keV allow us to probe several tens of nm into LAO-STO heterostructures. Our results establish that the presence of oxygen vacancy alone can quantitatively account for the doped charge carriers found in the Ti $3d$ band in the LAO/STO system. The distribution of charge carriers found in our experiments can account for many observations in these systems. Specifically, (i) our findings provide a natural explanation for experimental observations of charge carriers with very different mobilities and carrier concentrations reported for such samples depending on the experimental probe used, with the doped charges at the interface providing a relatively low carrier contribution with high mobility and the bulk doped carriers representing the lower mobility, but a much higher contribution to the total number of carriers in the system. (ii) These results also provide a natural explanation for the observed much larger spatial spread of the carrier distribution compared to the dimension of the interface. (iii) Samples produced with the aim to minimize oxygen vacancies tend to exhibit a charge-carrier concentration in the range 10^{12}–10^{13} cm^{-2}, which is $\sim$1–2 orders of magnitude smaller than the carrier concentration of $\sim 3\times10^{14}$ cm^{-2} predicted by the polar catastrophe model for a fully oxygenated sample (i.e., in the absence of anion vacancies); the doping of the interface with charge carriers in such a sample is possibly controlled by minute concentrations of oxygen vacancies still present on the LAO surface populating the lowest energy states available at the interface due to band bending.

ACKNOWLEDGMENTS

Financial support by the Department of Science & Technology (Government of India) provided within the framework of the India@DESY collaboration, and by the Swedish Foundation for International Cooperation in Research and Higher Education (STINT), are gratefully acknowledged.

[1] A. Ohtomo and H. Y. Hwang, Nature (London) **427**, 423 (2004).
[2] S. Thiel, G. Hammerl, A. Schmehl, C. W. Schneider, and J. Mannhart, Science **313**, 1942 (2006).
[3] H. Y. Hwang, Y. Iwasa, M. Kawasaki, B. Keimer, N. Nagaosa, and Y. Tokura, Nat. Mater. **11**, 103 (2012).
[4] M. Huijben, A. Brinkman, G. Koster, G. Rijnders, H. Hilgenkamp, and D. H. A. Blank, Adv. Mater. **21**, 1665 (2009).
[5] N. Reyren, S. Thiel, A. D. Caviglia, L. F. Kourkoutis, G. Hammerl, C. Richter, C. W. Schneider, T. Kopp, A.-S. Rüetschi, D. Jaccard, M. Gabay, D. A. Muller, J.-M. Triscone, and J. Mannhart, Science **317**, 1196 (2007).
[6] A. D. Caviglia, S. Gariglio, N. Reyren, D. Jaccard, T. Schneider, M. Gabay, S. Thiel, G. Hammerl, J. Mannhart, and J. M. Triscone, Nature (London) **456**, 624 (2008).

[7] A. Brinkman, M. Huijben, M. van Zalk, J. Huijben, U. Zeitler, J. C. Maan, W. G. van der Wiel, G. Rijnders, D. H. A. Blank, and H. Hilgenkamp, Nat. Mater. **6**, 493 (2007).

[8] J. A. Bert, B. Kalisky, C. Bell, M. Kim, Y. Hikita, H. Y. Hwang, and K. A. Moler, Nat. Phys. **7**, 767 (2011).

[9] J. S. Lee, Y. W. Xie, H. K. Sato, C. Bell, Y. Hikita, H. Y. Hwang, and C. C. Kao, Nat. Mater. **12**, 703 (2013).

[10] A. D. Caviglia, S. Gariglio, C. Cancellieri, B. Sacépé, A. Fête, N. Reyren, M. Gabay, A. F. Morpurgo, and J. M. Triscone, Phys. Rev. Lett. **105**, 236802 (2010).

[11] M. Ben Shalom, A. Ron, A. Palevski, and Y. Dagan, Phys. Rev. Lett. **105**, 206401 (2010).

[12] N. Nakagawa, H. Y. Hwang, and D. A. Muller, Nat. Mater. **5**, 204 (2006).

[13] S. Okamoto, A. J. Millis, and N. A. Spaldin, Phys. Rev. Lett. **97**, 056802 (2006).

[14] W. Siemons, G. Koster, H. Yamamoto, W. A. Harrison, G. Lucovsky, T. H. Geballe, D. H. A. Blank, and M. R. Beasley, Phys. Rev. Lett. **98**, 196802 (2007).

[15] Y. Chen, N. Pryds, J. E. Kleibeuker, G. Koster, J. Sun, E. Stamate, B. Shen, G. Rijnders, and S. Linderoth, Nano Lett. **11**, 3774 (2011).

[16] G. Herranz, F. Sánchez, N. Dix, M. Scigaj, and J. Fontcuberta, Sci. Rep. **2**, 758 (2012).

[17] G. Herranz, M. Basletić, M. Bibes, C. Carrétéro, E. Tafra, E. Jacquet, K. Bouzehouane, C. Deranlot, A. Hamzić, J.-M. Broto, A. Barthélémy, and A. Fert, Phys. Rev. Lett. **98**, 216803 (2007).

[18] Z. S. Popović, S. Satpathy, and R. M. Martin, Phys. Rev. Lett. **101**, 256801 (2008).

[19] P. R. Willmott, S. A. Pauli, R. Herger, C. M. Schlepütz, D. Martoccia, B. D. Patterson, B. Delley, R. Clarke, D. Kumah, C. Cionca, and Y. Yacoby, Phys. Rev. Lett. **99**, 155502 (2007).

[20] E. Breckenfeld, N. Bronn, J. Karthik, A. R. Damodaran, S. Lee, N. Mason, and L. W. Martin, Phys. Rev. Lett. **110**, 196804 (2013).

[21] K. Yoshimatsu, R. Yasuhara, H. Kumigashira, and M. Oshima, Phys. Rev. Lett. **101**, 026802 (2008).

[22] D. A. Dikin, M. Mehta, C. W. Bark, C. M. Folkman, C. B. Eom, and V. Chandrasekhar, Phys. Rev. Lett. **107**, 056802 (2011).

[23] G. Berner, M. Sing, H. Fujiwara, A. Yasui, Y. Saitoh, A. Yamasaki, Y. Nishitani, A. Sekiyama, N. Pavlenko, T. Kopp, C. Richter, J. Mannhart, S. Suga, and R. Claessen, Phys. Rev. Lett. **110**, 247601 (2013).

[24] W.-j. Son, E. Cho, B. Lee, J. Lee, and S. Han, Phys. Rev. B **79**, 245411 (2009).

[25] A. Janotti, L. Bjaalie, L. Gordon, and C. G. Van de Walle, Phys. Rev. B **86**, 241108 (2012).

[26] M. Basletic, J. L. Maurice, C. Carretero, G. Herranz, O. Copie, M. Bibes, E. Jacquet, K. Bouzehouane, S. Fusil, and A. Barthelemy, Nat. Mater. **7**, 621 (2008).

[27] N. Reyren, S. Gariglio, A. D. Caviglia, D. Jaccard, T. Schneider, and J. M. Triscone, Appl. Phys. Lett. **94**, 112506 (2009).

[28] M. Sing, G. Berner, K. Goß, A. Müller, A. Ruff, A. Wetscherek, S. Thiel, J. Mannhart, S. A. Pauli, C. W. Schneider, P. R. Willmott, M. Gorgoi, F. Schäfers, and R. Claessen, Phys. Rev. Lett. **102**, 176805 (2009).

[29] O. Copie, V. Garcia, C. Bödefeld, C. Carrétéro, M. Bibes, G. Herranz, E. Jacquet, J. L. Maurice, B. Vinter, S. Fusil, K. Bouzehouane, H. Jaffrès, and A. Barthélémy, Phys. Rev. Lett. **102**, 216804 (2009).

[30] A. Dubroka, M. Rössle, K. W. Kim, V. K. Malik, L. Schultz, S. Thiel, C. W. Schneider, J. Mannhart, G. Herranz, O. Copie, M. Bibes, A. Barthélémy, and C. Bernhard, Phys. Rev. Lett. **104**, 156807 (2010).

[31] K. Janicka, J. P. Velev, and E. Y. Tsymbal, Phys. Rev. Lett. **102**, 106803 (2009).

[32] T. Fix, F. Schoofs, J. L. MacManus-Driscoll, and M. G. Blamire, Phys. Rev. Lett. **103**, 166802 (2009).

[33] K. J. Zhou, M. Radovic, J. Schlappa, V. Strocov, R. Frison, J. Mesot, L. Patthey, and T. Schmitt, Phys. Rev. B **83**, 201402 (2011).

[34] V. K. Guduru, A. Granados del Aguila, S. Wenderich, M. K. Kruize, A. McCollam, P. C. M. Christianen, U. Zeitler, A. Brinkman, G. Rijnders, H. Hilgenkamp, and J. C. Maan, Appl. Phys. Lett. **102**, 051604 (2013).

[35] S. S. A. Seo, Z. Marton, W. S. Choi, G. W. J. Hassink, D. H. A. Blank, H. Y. Hwang, T. W. Noh, T. Egami, and H. N. Lee, Appl. Phys. Lett. **95**, 082107 (2009).

[36] N. Pavlenko, T. Kopp, E. Y. Tsymbal, G. A. Sawatzky, and J. Mannhart, Phys. Rev. B **85**, 020407 (2012).

[37] C. Bell, S. Harashima, Y. Kozuka, M. Kim, B. G. Kim, Y. Hikita, and H. Y. Hwang, Phys. Rev. Lett. **103**, 226802 (2009).

[38] A. Joshua, S. Pecker, J. Ruhman, E. Altman, and S. Ilani, Nat. Commun. **3**, 1129 (2012).

[39] M. Salluzzo, J. C. Cezar, N. B. Brookes, V. Bisogni, G. M. De Luca, C. Richter, S. Thiel, J. Mannhart, M. Huijben, A. Brinkman, G. Rijnders, and G. Ghiringhelli, Phys. Rev. Lett. **102**, 166804 (2009).

[40] P. Delugas, A. Filippetti, V. Fiorentini, D. I. Bilc, D. Fontaine, and P. Ghosez, Phys. Rev. Lett. **106**, 166807 (2011).

[41] S. Mukherjee, A. Hazarika, P. K. Santra, A. L. Abdelhady, M. A. Malik, M. Gorgoi, P. O'Brien, O. Karis, and D. D. Sarma, J. Phys. Chem. C **118**, 15534 (2014).

[42] S. Mukherjee, R. Knut, S. M. Mohseni, T. N. Anh Nguyen, S. Chung, Q. Tuan Le, J. Åkerman, J. Persson, A. Sahoo, A. Hazarika, B. Pal, S. Thiess, M. Gorgoi, P. S. Anil Kumar, W. Drube, O. Karis, and D. D. Sarma, Phys. Rev. B **91**, 085311 (2015).

[43] R. Claessen, M. Sing, M. Paul, G. Berner, A. Wetscherek, A. Müller, and W. Drube, New J. Phys. **11**, 125007 (2009), part of Focus on Advances in Surface and Interface Science 2009 .

[44] M. Gorgoi, S. Svensson, F. Schäfers, G. Öhrwall, M. Mertin, P. Bressler, O. Karis, H. Siegbahn, A. Sandell, H. Rensmo, W. Doherty, C. Jung, W. Braun, and W. Eberhardt, Nucl. Instrum. Methods Phys. Res., Sec. A **601**, 48 (2009).

[45] S. Granroth, R. Knut, M. Marcellini, G. Andersson, S. Svensson, O. Karis, M. Gorgoi, F. Schäfers, W. Braun, W. Eberhardt, W. Olovsson, E. Holmström, and N. Mårtensson, Phys. Rev. B **80**, 094104 (2009).

[46] X. Kozina, S. Ouardi, B. Balke, G. Stryganyuk, G. H. Fecher, C. Felser, S. Ikeda, H. Ohno, and E. Ikenaga, Appl. Phys. Lett. **96**, 072105 (2010).

[47] M. Takizawa, S. Tsuda, T. Susaki, H. Y. Hwang, and A. Fujimori, Phys. Rev. B **84**, 245124 (2011).

[48] C. Cancellieri, M. L. Reinle-Schmitt, M. Kobayashi, V. N. Strocov, T. Schmitt, P. R. Willmott, S. Gariglio, and J.-M. Triscone, Phys. Rev. Lett. **110**, 137601 (2013).

[49] C. Bell, S. Harashima, Y. Hikita, and H. Y. Hwang, Appl. Phys. Lett. **94**, 222111 (2009).

[50] F. Schaefers, M. Mertin, and M. Gorgoi, Rev. Sci. Instrum. **78**, 123102 (2007).

[51] Y. Takata, Y. Kayanuma, M. Yabashi, K. Tamasaku, Y. Nishino, D. Miwa, Y. Harada, K. Horiba, S. Shin, S. Tanaka, E. Ikenaga, K. Kobayashi, Y. Senba, H. Ohashi, and T. Ishikawa, Phys. Rev. B **75**, 233404 (2007).

[52] D. D. Sarma, P. K. Santra, S. Mukherjee, and A. Nag, Chem. Mater. **25**, 1222 (2013).

[53] P. K. Santra, R. Viswanatha, S. M. Daniels, N. L. Pickett, J. M. Smith, P. O'Brien, and D. D. Sarma, J. Am. Chem. Soc. **131**, 470 (2009).

[54] We note that 6 uc of LAO has a thickness of 2.27 nm against the 2.75 nm deduced here. This arises from the uncertainty in determining λ. Since the spectroscopic intensities are a function of only d/λ, the thickness d can be easily made to match with a slight adjustment of λ used. However, we prefer to compute λ from the standard procedure [66] and use the same with its uncertainty, rather than use it as an adjustable parameter.

[55] E. Slooten, Z. Zhong, H. J. A. Molegraaf, P. D. Eerkes, S. de Jong, F. Massee, E. van Heumen, M. K. Kruize, S. Wenderich, J. E. Kleibeuker, M. Gorgoi, H. Hilgenkamp, A. Brinkman, M. Huijben, G. Rijnders, D. H. A. Blank, G. Koster, P. J. Kelly, and M. S. Golden, Phys. Rev. B **87**, 085128 (2013).

[56] We have explored different functional forms of the charge-carrier distribution, such as Gaussian, rectangular, and triangular forms, at the interface or away from the interface, but a single charge-carrier distribution was always found to be inadequate in describing the experimental Ti^{3+}/Ti^{4+} intensity ratio as a function of photon energy for both 6L and 4L samples.

[57] W. Meevasana, P. D. C. King, R. H. He, S. K. Mo, M. Hashimoto, A. Tamai, P. Songsiriritthigul, F. Baumberger, and Z. X. Shen, Nat. Mater. **10**, 114 (2011).

[58] G. Khalsa and A. H. MacDonald, Phys. Rev. B **86**, 125121 (2012).

[59] K. Ueno, S. Nakamura, H. Shimotani, A. Ohtomo, N. Kimura, T. Nojima, H. Aoki, Y. Iwasa, and M. Kawasaki, Nat. Mater. **7**, 855 (2008).

[60] A. F. Santander-Syro, O. Copie, T. Kondo, F. Fortuna, S. Pailhes, R. Weht, X. G. Qiu, F. Bertran, A. Nicolaou, A. Taleb-Ibrahimi, P. Le Fevre, G. Herranz, M. Bibes, N. Reyren, Y. Apertet, P. Lecoeur, A. Barthelemy, and M. J. Rozenberg, Nature (London) **469**, 189 (2011).

[61] The probing depth in our measurements does not allow us to quantify beyond that depth.

[62] J. N. Eckstein, Nat. Mater. **6**, 473 (2007).

[63] Z. Q. Liu, C. J. Li, W. M. Lü, X. H. Huang, Z. Huang, S. W. Zeng, X. P. Qiu, L. S. Huang, A. Annadi, J. S. Chen, J. M. D. Coey, T. Venkatesan, and Ariando, Phys. Rev. X **3**, 021010 (2013).

[64] N. C. Bristowe, P. B. Littlewood, and E. Artacho, Phys. Rev. B **83**, 205405 (2011).

[65] Y. Li, S. N. Phattalung, S. Limpijumnong, J. Kim, and J. Yu, Phys. Rev. B **84**, 245307 (2011).

[66] S. Tanuma, C. J. Powell, and D. R. Penn, Surf. Interface Anal. **35**, 268 (2003).